

Pressure induced electronic band evolution and observation of superconductivity in the Dirac semimetal ZrTe₅

Sanskar Mishra¹, Nagendra Singh¹, Vinod K. Gangwar², Rajan Walia³, Jianping Sun⁴, Genfu Chen⁴, Dilip Bhoi⁵, Sandip Chatterjee⁶, Yoshiya Uwatoko⁵, Jinguang Cheng^{4†}, Prashant Shahi^{1*}

¹*Department of Physics, Deen Dayal Upadhyaya Gorakhpur University, Gorakhpur, 273009, India*

²*Department of Physics, K.G.K. (P.G.) College, Moradabad, 244001, India*

³*Department of Physics, University of Allahabad, Prayagraj, 211002, India*

⁴*Beijing National Laboratory for Condensed Matter Physics and Institute of Physics, Chinese Academy of Sciences, Beijing, 100190 China*

⁵*Institute for Solid State Physics, University of Tokyo, Kashiwa, Chiba 277-8581, Japan*

⁶*Department of Physics, Indian institute of technology (IIT)-BHU, Varanasi, 221005, India*

(Dated: February 10, 2026)

We report a comprehensive investigation of the pressure effects on the magnetotransport properties of the topological material ZrTe₅ within 1–8 GPa pressure range. With increasing pressure, the characteristic peak (T_p) in its electrical resistivity $\rho(T)$ first shifts to higher temperature and then moves quickly towards the lower temperature before disappearing eventually at 6 GPa. Beyond 6 GPa, the system exhibits metallic behavior across the entire temperature range, and superconductivity emerges below $T_c = 1.8$ K at 8 GPa. Based on the systematic magnetotransport measurement under pressure, we demonstrate that the superconductivity occurs following a significant electronic structure modulation possibly due to pressure induced structural changes near 6 GPa, which coincides with dramatic enhancement of the magnetoresistance (MR) reaching up to $\sim 1400\%$. Our experimental results are substantiated by density functional theory calculations as the application of pressure drastically alters the density of states near the Fermi level. Notably, multiple hole pockets emerge at the Fermi level from 4 GPa onward, and their contributions are further enhanced with increasing pressure. The combined experimental and theoretical investigation reveals a comprehensive evolution of electronic structure of Dirac semimetal ZrTe₅ under pressure and suggest a possible link between the Fermi surface reconstruction in the pressure range of structural transition and emergence of superconductivity.

I. INTRODUCTION

Pressure-driven superconductivity in topologically non-trivial materials continues to attract considerable attention, particularly for its feasibility in realizing topological superconductivity (TSC)[1]. Variety of topological materials have been explored in this context, including topological insulators (e.g., Bi₂Te₃, Bi₂Se₃) [2–5] and Dirac/Weyl semimetals (e.g., Cd₃As₂, WTe₂, MoTe₂) [6–8], which highlights the relevance of high-pressure studies in the search for unconventional superconducting states. In general, pressure-induced superconductivity in the topological systems is often a consequence of lattice or electronic instability induced by pressure, manifested as structural transitions or significant anomalies in the physical properties. For instance, superconductivity emerges in topological insulator Bi₂Te₃ upon compression up to 3.2 GPa, where the slope of Hall coefficient (dR_H/dP) exhibits a pronounced change [2–5]. In the Dirac semimetal Cd₃As₂, the structural transition takes place near 3 GPa, prior to the appearance of superconductivity at 8.5 GPa [6], and the symmetry breaking associated with the structural distortion has been proposed to be favorable for realizing topological superconductivity [9]. The emergence of superconductivity in the Weyl

semimetal WTe₂ at 10.5 GPa coincides with the complete suppression of its extreme magnetoresistance (XMR) and sign reversal of Hall coefficient (R_H) [7]. In contrast, superconductivity emerges in NbAs₂ before the XMR is completely suppressed, as the pressure modifies Fermi surface while maintaining the electron-hole compensation [10]. Furthermore, unconventional superconductivity has also been reported in several other topological semimetals such as LaBi [11] and MoP [12, 13], for which electronic instabilities were found to be essential for realizing this state. Therefore, the application of high pressure can be employed as an effective approach to induce superconductivity by regulating the structural and/or electronic properties of topological materials.

Zirconium pentatelluride (ZrTe₅) is an established topological material with Dirac-like band dispersion [14] and exhibits numerous unusual properties associated with its peculiar electronic states, including resistivity anomaly [15, 16], chiral magnetic effect [17], anomalous Hall effect (AHE) [18], anomalous thermoelectric effect [19, 20], magneto chiral anisotropy [21] etc. Previous studies have shown a significant effect of pressure on its electronic structure, leading to pressure-induced topological [22–24] and superconducting [25] transitions. Recently, we investigated the thermoelectric and magnetotransport properties of ZrTe₅ single crystals under hydrostatic pressure up to 2 GPa [26], and observed an upward shift of its characteristic resistivity peak towards higher temperatures with pressure. The magnetotrans-

* prashant.phy@ddugu.ac.in; † jgcheng@iphy.ac.cn

port studies under hydrostatic pressure also reveals a phase change in quantum oscillations around ~ 2 GPa, suggesting pressure induced modification in Fermi surface topology similar to the report from other group [27]. Additionally, our previous study also revealed that the application of moderate pressure enhances simultaneously resistivity $\rho(T)$ and thermopower $S(T)$, leading to a significant enhancement of the thermoelectric power factors at room temperature [26]. These results clearly suggest that the application of pressure can significantly tune the electronic structure of ZrTe_5 even in low pressure regime (0-2 GPa). High pressure studies reaching up to ~ 50 GPa in $\text{ZrTe}_5/\text{HfTe}_5$ have been reported by several groups, where a semimetal to superconducting transition associated with structural phase transition have been observed near 6 GPa [23, 25, 28, 29], with the superconducting critical temperature T_c increases up to ~ 6 K at higher pressure. These studies establish a link between the structural transition and superconductivity, though the precise pressure at which this transition occurs can vary between different crystal batches owing to the well-known sensitivity of the transport properties of ZrTe_5 to the crystal growth method. While the past studies have primarily aimed at investigation of topological phase transition in low pressure regime or the observation of superconductivity at elevated pressures, a detailed understanding on evolution of electronic properties in the intermediate pressure range remain limited. In particular, evolutions of MR, Hall resistivity (ρ_{xy}), resistivity peak (T_p), and the electronic structure as function of pressure have not been adequately studied.

Therefore, in the present study, we have systematically investigated the magnetotransport properties of chemical vapor transport (CVT) grown ZrTe_5 single crystals under various hydrostatic pressures from 1 to 8 GPa in order to complement and extend the existing high pressure studies of transition metal pentatellurides (ZrTe_5). Our results confirmed a significant effect of pressure on the electrical transport properties of ZrTe_5 . Notably, the characteristic resistivity peak (T_p) displays a pronounced non-monotonic pressure dependence, which initially increases with pressure and then shifts towards lower temperature before ultimately vanishes near 6 GPa. The superconducting transition with $T_c = 1.8$ K was observed to occur at 8 GPa. The magnetotransport results (MR and Hall resistivity) provide systematic band evolution under pressure. The transition in bands from electron-like to hole-like began at 4 GPa, as evidenced by the emergence of significant non-linearity in MR and Hall data consistent with the DFT calculations. At 6 GPa, a perfect balance between the two type of carriers is achieved marked by a dramatic increase in the low-temperature MR ($\sim 1400\%$ at 8 T). In contrast with other topological materials, we observed distinctive non-monotonic pressure dependence of MR in ZrTe_5 , e.g. MR first decreases sharply in the low-pressures regime (down to $\sim 50\%$ at 2 GPa), recovers in the intermediate pressure range (200% at 3-5 GPa), and then rises sharply at 6 GPa ($\sim 1400\%$) along with the

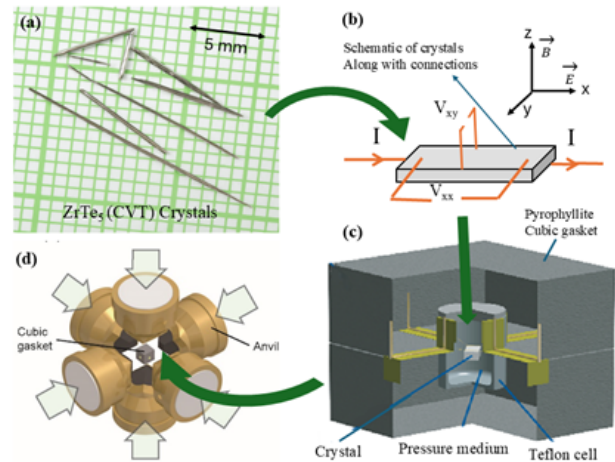


Figure 1. (a) Optical image of CVT grown ZrTe_5 single crystals. (b) Illustration of four probe measurement of transport properties under applied magnetic field B . (c) Schematic views of the sample assembly inside the pyrophyllite cubic gasket. (d) Six anvils compressing the cubic gasket shown in figure (c). Panels (c,d) have been adapted from previous work of our group ref.[30, 31].

complete sign reversal of Hall resistivity. Our experimental observations are supported by first-principles DFT calculations, which display pressure-induced changes in calculated density of states (DOS) and band structures in the 1-6 GPa pressure range. Our results demonstrate that pressure plays a significant role in tuning properties of ZrTe_5 , likely through a pressure-induced structural transition and/or associated electronic reconstruction.

II. EXPERIMENTAL DETAILS

The ZrTe_5 single crystals used in this study were grown by the CVT technique [15, 16]. Structural and compositional characterizations together with the physical properties at the ambient pressure of these single crystals have been reported in our previous work [32]. A palm-type cubic anvil Pressure cell (PCAC) was used to measure magnetoresistance under hydrostatic pressures up to 8 GPa. The conventional four probe method was employed in resistivity measurement, where the direction of current was kept along ' a ' axis. In the magnetotransport measurements the direction of magnetic field was kept along ' b ' axis. For the generation of hydrostatic pressure, glycerol was used as the pressure-transmitting medium inside the pressure cell. Glycerol offers better hydrostaticity at low temperature in the intermediate pressure regime compared to other alternatives such as Daphne 7373 [33]. The pressure inside the cell was determined by the superconducting transition of lead (Pb) at low temperatures. Figure 1(a) presents the optical image of the CVT grown ZrTe_5 single crystals which has been reproduced

from our previous study [26]. Figure 1(b) illustrates the schematic of four probe measurement configuration for the magneto-transport experiments under applied magnetic field B . Figure 1(c, d) illustrates the pyrophyllite gasket along with the Teflon cell assembly in the center of PCAC, which are reproduced from our previous work [30, 31].

The electronic band structure and density of states (DOS) were computed using Quantum espresso package [34]. Generalized Gradient Approximation (GGA) was implemented using Perdew-Burke-Ernzerhof (PBE) functional [35] to account for exchange correlation effects. Additionally, we have also used Grimme's D3 dispersion correction [36] to account for van der Waal's interaction between different layers of ZrTe_5 . The convergence criteria were set for the force threshold to 10^{-5} atomic unit and for energy it is 10^{-12} Ry. The pressure convergence was maintained within 0.05 kbar. For these calculations, scalar-relativistic ultra-soft pseudopotentials were used. Spin-orbit coupling (SOC) has been considered while calculating bands and DOS. Furthermore, band structure has been calculated taking a $15 \times 15 \times 4$ k-point mesh, whereas a denser k-point mesh (double of the original one) has been used for non-self-consistent field (nscf) calculation to accurately map the Fermi level of the system.

III. RESULTS

A. Electrical resistivity under Pressure

Figure 2 presents the temperature dependence of electrical resistivity $\rho(T)$ at various pressures ($0 \leq P \leq 8$) for the ZrTe_5 crystals. At ambient pressure, $\rho(T)$ exhibits a broad peak at $T_p \sim 127$ K. This resistivity peak is a characteristic of CVT-grown ZrTe_5 crystals and is found to be associated with sign change of the Hall coefficient and thermopower, indicates a change of the dominant charge carriers from electrons (n-type) to holes (p-type) [16]. Using high-resolution angle-resolved photoemission spectroscopy (ARPES), previous studies have attributed this peak to a temperature-induced Lifshitz transition, where the electronic bands evolve from p-type semiconducting to n-type semimetallic behavior as the temperature decreases [37]. With increasing pressure, T_p initially shifts to higher temperature, reaching ~ 155 K at 1 GPa. Beyond this pressure, T_p decreases progressively, reaching as low as 38 K at 5 GPa, where a slight upturn like feature is observed below 15 K. Along with the downward shift of T_p , $\rho(T_p)$ changes moderately up to 4 GPa and then decreases by about an order of magnitude at 5 GPa. The pressure-driven evolution of T_p is consistent with previous studies on ZrTe_5 and its sister compound HfTe_5 [25, 38]. The initial increase in $\rho(T_p)$ with pressure can be attributed to the enlarged band gap, while its subsequent decrease beyond 4 GPa signals band gap closure an interpretation supported by recent density functional theory calculation [39]. At 6 GPa, the resistivity

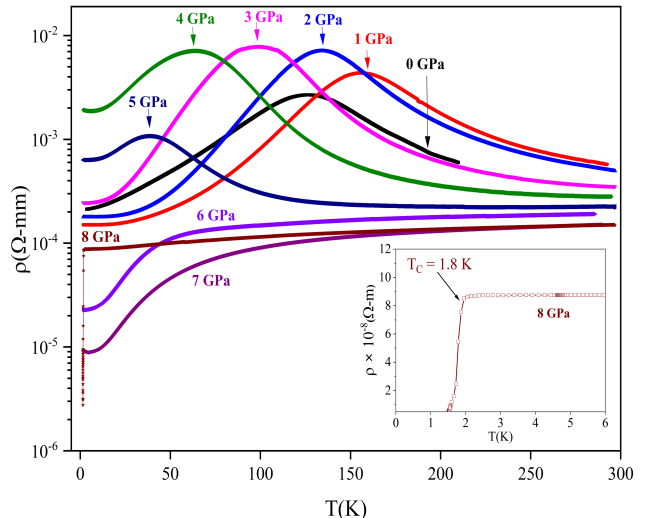


Figure 2. Temperature dependence of resistivity along a-axis of ZrTe_5 single crystals under various pressures up to 8 GPa. The application of pressure induces a notable change in resistivity peak (T_p and $\rho(T_p)$). The inset figure presents the low-temperature resistivity at 8 GPa, showcasing the superconducting transition at 1.8 K.

peak disappears completely, and a weak metallic character emerges in the temperature range of $50 \leq T \leq 300$ K. Below ~ 50 K, the resistivity exhibits a quick reduction, resulting in a residual resistivity $\rho(1.5 \text{ K})$ approximately 10 times lower than that at ambient pressure. The drastic change in the $\rho(T)$ curve profile at 6 GPa suggests significant alterations in the DOS near the Fermi level. At 7 GPa, the resistivity behavior is similar to that at 6 GPa, with only a slight reduction in overall magnitude. Upon further compression to 8 GPa, $\rho(T)$ curve change to a typical metallic behavior with weak temperature dependence in a wide temperature range, followed by a sudden drop at $T \sim 1.8$ K, inset of Fig. 2, due to the occurrence of the superconducting transition, which aligns with previous reports in pentatelluride systems [23, 25, 28].

B. Magnetotransport properties under pressure

1. Magnetoresistance (MR) under pressure

We investigated the evolution of longitudinal magnetoresistance (MR) of ZrTe_5 under varying pressure and temperature up to 8 GPa. The MR % was derived from the longitudinal resistance (R_{xx}) using the conventional formula as-

$$\text{MR}\% = \left(\frac{R_{xx}(B) - R_{xx}(0)}{R_{xx}(0)} \right) \times 100\% \quad (1)$$

where, $R_{xx}(B)$ and $R_{xx}(0)$ represent the longitudinal resistance in the presence and absence of a magnetic field,

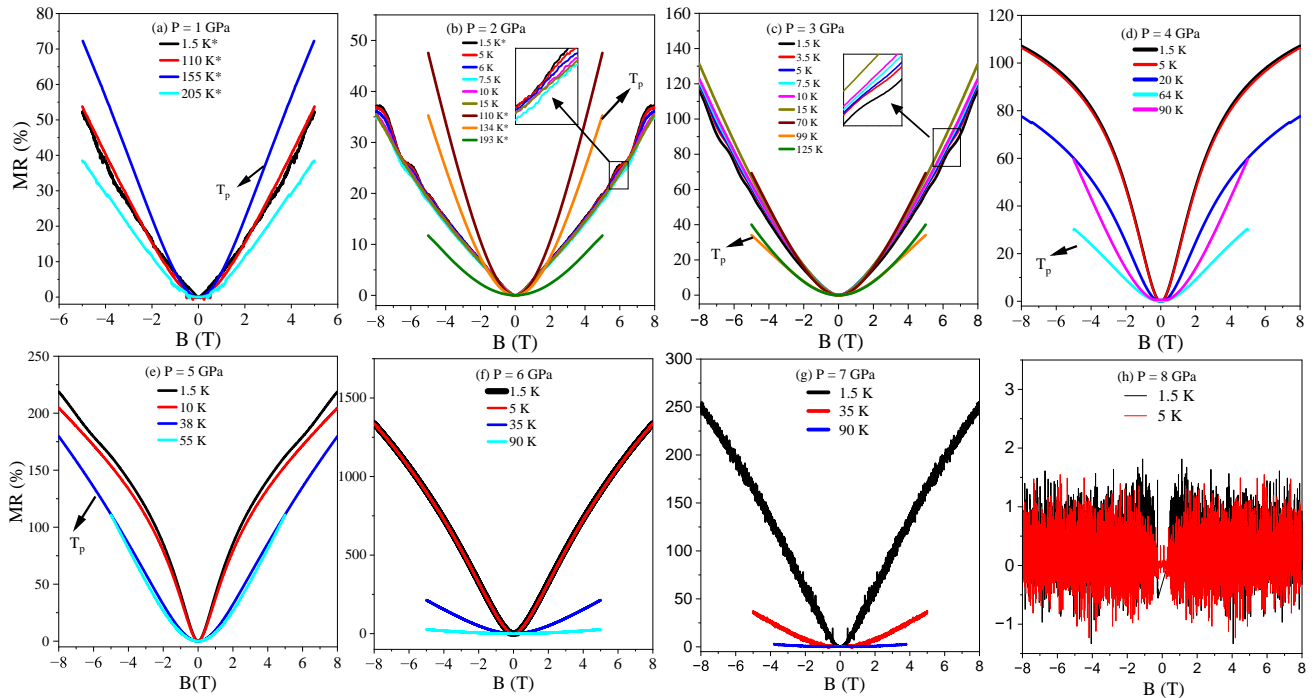


Figure 3. (a)–(h) Magnetic field dependence of magnetoresistance (MR %) of ZrTe₅ at varying pressures (1–8 GPa). In panels (b) and (c), pronounced SdH oscillations are observed at low temperatures. The insets of panels (b) and (c) show magnified views of the overlapping data. At 8 GPa (panel h), the MR signal exhibits noticeable degradation, likely arising from experimental constraints associated with the palm cubic anvil cell at high pressure. Asterisks (*) next to temperatures at 1 and 2 GPa indicate data reproduced from our recent study [26], included here for completeness.

respectively. Figure 3 displays the MR % as a function of magnetic field between 1–8 GPa pressure. At lower pressures ($P \leq 3$ GPa), the MR exhibits an almost linear, non-saturating field dependence, with a typical variation of $\text{MR} \propto B^{1-3}$, as shown in Fig. 3 (a)–(c). However, upon increasing the pressure beyond 3 GPa, it begins to deviate from the linear nature, displaying a saturation-like tendency at higher magnetic fields, approximately following $\text{MR} \propto B^{0.9}$ [Fig. 3(d)–(f)]. At 8 GPa [Fig. 3(h)], the MR signal exhibits noticeable degradation, which may be attributed to the reduced signal magnitude under extreme pressure conditions and possible experimental constraints related to the high-pressure cell or the pressure-transmitting medium.

At lower field in the 4–6 GPa pressure range, the variation of MR is much steeper with cusp V-shaped features below T_p , which may tentatively be associated with spin dependent scattering mechanism as pressure may strengthen the spin orbit interaction. Remarkably, at 6 GPa there is dramatic enhancement in MR reaching as high as ~ 1400 % at low temperature and 8 T magnetic field [Fig. 3(f)]. Such a huge MR implies a substantial modification in the electronic band structure of the system. As the pressure is raised, the MR near T_p also varies systematically, i.e. it is the highest at 1 GPa, intermediate at 2 GPa and becomes significantly suppressed beyond 3 GPa. A comparison to our previous ambient

pressure study of ZrTe₅ samples of the same batch [32] reveals a significant suppression of MR by pressure, similar as those reported by other groups [27]. It should be noted that at pressures of 2 and 3 GPa, pronounced Shubnikov de Haas (SdH) oscillations can be observed in MR curves at low temperatures, which we have discussed in detail in our recent study [26].

2. Hall Resistivity (ρ_{xy}) under pressure

To obtain the carrier information involved in pressure-dependent transport phenomenon, we measured the Hall resistivity (ρ_{xy}) as functions of magnetic field at various temperatures and pressures [Figure 4]. Up to 5 GPa, where T_p exists, the observed negative slope at $T < T_p$ of ρ_{xy} reflects the dominance of electrons as the majority carrier. However, above T_p , the slope changes to positive, indicating a switch to hole dominated charge transport. At T_p , where both electron and hole coexist, the ρ_{xy} curve becomes relatively flat, highlighting the contribution of both carrier types. In 4–6 GPa pressure range, a pronounced curvature in $\rho_{xy}(B)$ emerges and this feature becomes prominent with pressure. Remarkably, the initial slope of $\rho_{xy}(B)$ at low temperatures changes from negative to positive between 5 and 6 GPa, signaling a switch in the dominant carrier type from electron to hole-like. Furthermore, based on the increasing non-linearity

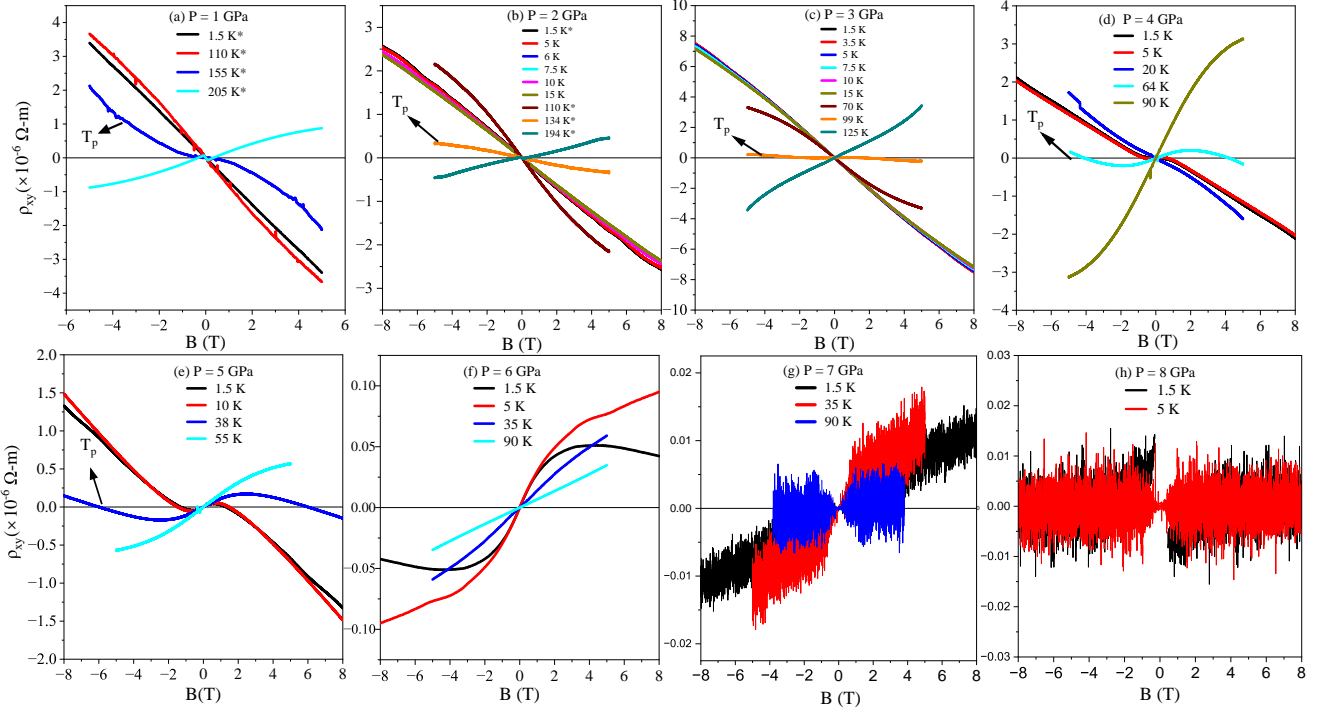


Figure 4. (a)–(h) Magnetic field dependence of the Hall resistivity (ρ_{xy}) of ZrTe₅ under varying pressures up to 8 GPa. In the low-pressure regime (1–3 GPa), ρ_{xy} varies nearly linearly with magnetic field (a–c). In the intermediate-pressure regime (4–6 GPa), ρ_{xy} exhibits pronounced non-linear behavior, accompanied by a complete sign reversal at 6 GPa (d–f). In the high-pressure regime (7–8 GPa), the ρ_{xy} signal shows noticeable degradation due to the reduced Hall voltage under extreme pressure conditions (g–h); nevertheless, the Hall sign reversal clearly persists up to 7 GPa. Asterisks (*) next to temperatures at 1 and 2 GPa indicate data reproduced from our recent study [26].

in MR and Hall, we estimated the charge carrier density (n) and mobility (μ) by fitting the Hall conductivity (σ_{xy}) using two band model, given in Figure 5 & 6. Here, the Hall conductivity can be calculated from the resistivity tensor as $\sigma_{xy} = \frac{\rho_{xy}}{\rho_{xx}^2 + \rho_{xy}^2}$, where $\rho_{xx(xy)}$ is the longitudinal (Hall) resistivity. Using these values, the complete formula for Hall conductivity becomes-

$$\sigma_{xy} = \pm eB \left(\frac{n_1 \mu_1^2}{1 + \mu_1^2 B^2} + \frac{n_2 \mu_2^2}{1 + \mu_2^2 B^2} \right) \quad (2)$$

Here, n_1 and n_2 are the density, μ_1 and μ_2 are the mobility of two different types of carriers, and ‘ e ’ is fundamental electronic charge, and B is the applied magnetic field taken as independent variable. For each temperature and pressure, a magnetic field window 0-5 T was used to ensure the consistency in the procedure at for all measurement. The quality of these fits can be assessed via the σ_{xy} vs B curves provided in the Appendix C for all pressures at 1.5 K. The negative or positive sign is considered depending on whether the corresponding carriers are electrons or holes, respectively.

Figure 5 and 6 represents the estimated carrier density (n) and mobility (μ) at 1-3 and 4-6 GPa pressures respectively. The corresponding data at pressure 7 and

8 GPa is not shown here due to significant deterioration in signal quality. It is clear from Figure 5 that in the low-pressure regime (1-3 GPa) the conduction is predominantly electronic with carrier density $n \sim 10^{23}$ - 10^{24} m⁻³ below the peak temperature (T_p), while both electrons and holes participate in conduction near T_p , albeit with slightly lower densities. Above T_p , the hole density increases significantly and becomes nearly two order higher than that of electrons. At each pressure there is substantial redistribution of carriers is observed with increasing temperature, consistent with the temperature-induced Lifshitz transition as observed at ambient pressure [37, 40]. The higher mobility of electrons at 2 and 3 GPa leads to the pronounced Shubnikov-de Haas (SdH) quantum oscillations in MR as seen in Fig. 3 (b,c).

Upon further increasing pressure beyond 3 GPa the hole dominated conduction becomes more prominent. As shown in Figure 6, the higher mobility holes start appearing right from low temperature, in contrast with results shown in Figure 5. This observation suggests that the phenomenon of bipolar conduction which was typically confined near T_p at low pressures low (1-3 GPa, Fig. 5) persists throughout the entire temperature range because of pressure induced band modulations, and this extended

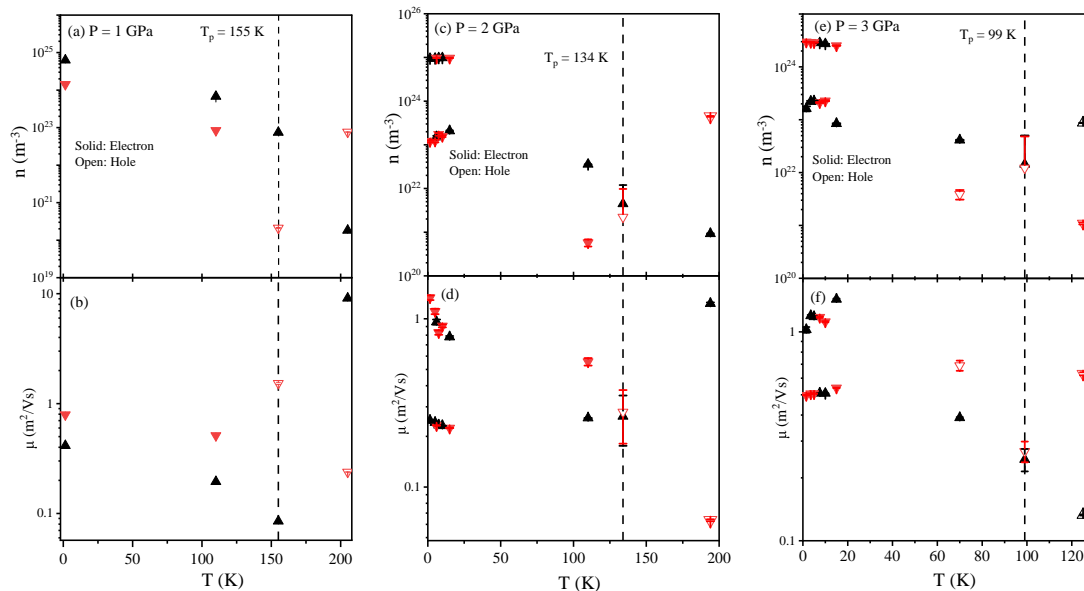


Figure 5. Temperature dependence of carrier density (n) (a, c, e) and mobility (μ) (b, d, f) at 1-3 GPa pressure. Here, the solid symbols have been used to denote electron while the open symbols represent holes.

bipolar conduction seems to be responsible for the enhanced $\rho(1.5\text{K})$ at 4 and 5 GPa [Figure 2]. Furthermore, Figure 6 shows that the contribution from holes keeps increasing with temperature at each pressure. In between 5 and 6 GPa, the band becomes increasingly hole-like as evidenced by the positive slope of ρ_{xy} at 6 GPa pressure [Fig. 4(f)]. At 6 GPa, the electrons with comparable density as holes appear at low temperatures, which causes the dramatic enhancement in MR $\sim 1400\%$ at magnetic field of 8 T. In addition, due to the linearity of ρ_{xy} and MR at $T = 35\text{ K}$ and 90 K two carriers model failed to fit the Hall conductivity reliably. The linearity of ρ_{xy} at 35 and 90 K (6 GPa) indicates that transport at these temperatures is dominated by a single type of charge carrier, namely holes. Multiple bands may still exist, but their contributions to the Hall signal are negligible. Thus, we applied one band model viz. $n = \frac{dB}{|e| d\rho_{xy}}$ and $\mu = \frac{1}{|e| n \rho_{xx}}$ which indicates the hole dominated transport with highest carrier density throughout the investigated pressure.

C. Electronic band structure and Density of states (DOS) under pressure

In Fig. 7(a), we show the two layers of ZrTe_5 extended in the ac -plane, which are stacked along the b -axis by weak van der Waals interactions, forming a 3D ZrTe_5 crystal. The interlayer bonding energy is as low as that between the layers of graphite [14]; therefore, it is highly sensitive to external perturbations such as pressure and strain. The Brillouin zone along with the high-symmetry points is shown in Fig. 7(b), where \mathbf{b}_1 , \mathbf{b}_2 , and \mathbf{b}_3 are

the reciprocal lattice vectors. Figure 7(c) displays the pressure dependence of the optimized lattice constants (a , b , and c) and the unit-cell volume from ambient to 6 GPa pressure. The calculated ambient-pressure lattice parameters, $a = 4.03476\text{ \AA}$, $b = 14.87163\text{ \AA}$, and $c = 13.6695\text{ \AA}$, are in good agreement with the experimentally reported values ($a = 3.9830\text{ \AA}$, $b = 14.87163\text{ \AA}$, and $c = 13.6695\text{ \AA}$) [32]. As we increase the pressure, all lattice parameters decrease unevenly, with the order $b > a > c$. Since the b -axis represents the interlayer spacing, pressure reduces the interlayer spacing of ZrTe_5 crystals to about 7 % of the original value at 6 GPa, which is also consistent with previously reported DFT calculations [39]. The calculated unit-cell volume shows a similar linear dependence on pressure as the lattice constants. At 6 GPa, it remains at approximately 85 % of its original value.

We computed the electronic band structure and density of states (DOS) by optimizing the atomic positions and lattice parameters of ZrTe_5 at different pressures up to 6 GPa [Figure 8]. The spin-orbit coupling (SOC) effects were considered for all these calculations. Figure 8(a) illustrates the density of states (DOS) at selected pressures of 1, 4 and 6 GPa. It is evident from this figure that as the pressure increases, there is a significant change in the DOS at the Fermi level notably, the states below the Fermi level are populated. Figures 8(b-d) show the band structures at 1, 4, and 6 GPa. The ambient pressure electronic bands and DOS have been discussed in detail in our recent study [26] and the data corresponding to 2, 3 and 5 GPa are given in Appendix D.

At ambient pressure, the valance band maxima (VBM)

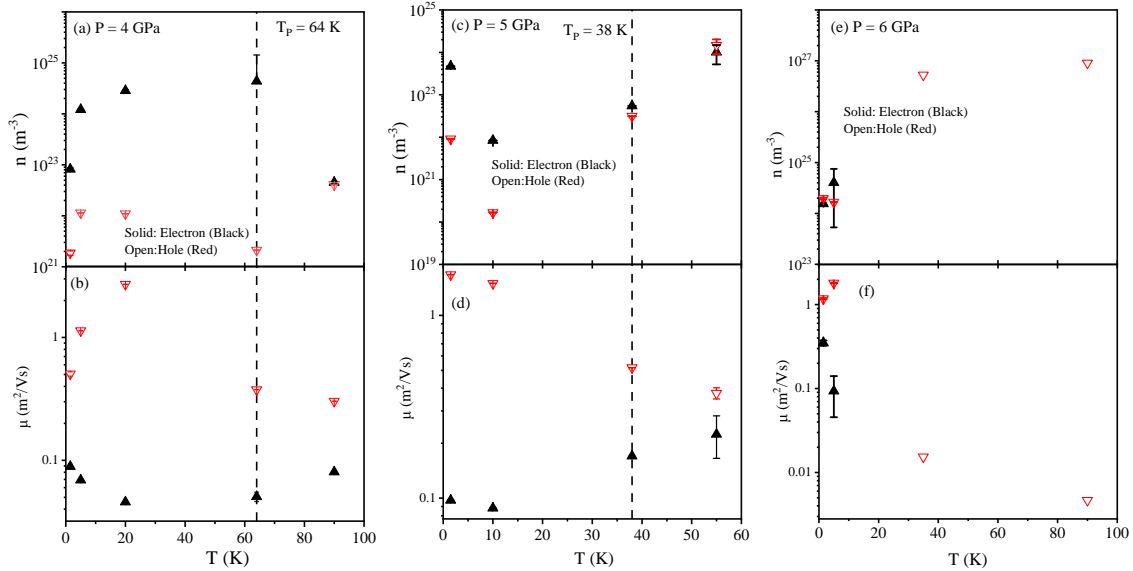


Figure 6. Temperature dependence of carrier density (n) (a, c, e) and mobility (μ) (b, d, f) at 4-6 GPa. Here, the solid symbols have been used to denote electron while the open symbols represent holes.

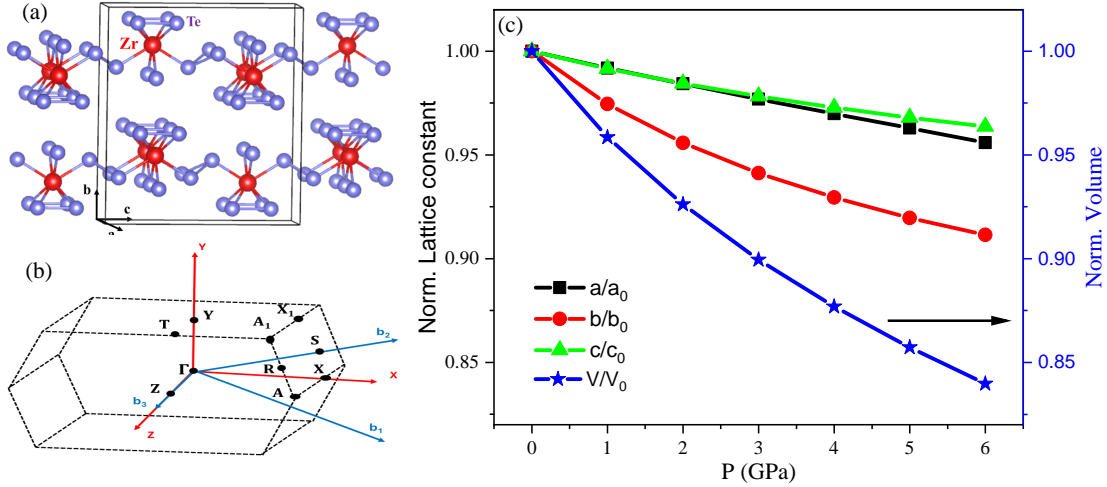


Figure 7. (a) Crystal structure of ZrTe₅ in which trigonal chains of ZrTe₃ run along the a axis and different chains are joined along the c axis by zig-zag Te atoms. In ac plane it forms 2D ZrTe₅, which are stacked along b axis by weak van der Waals forces. (b) Brillouin zone of ZrTe₅ with the high symmetry points along which band structure has been calculated. (c) Pressure dependent normalized lattice constants and volume of ZrTe₅ unit cell.

and conduction band minima (CBM) meet at the Fermi level forming Dirac like band dispersion at the Γ -point [26]. At 1 GPa, there is an opening of the band gap at the Γ point. In this case, the CBM and VBM shifts along Γ -Y direction with $\Delta \sim 70$ meV, Fig. 8(b). As the pressure increases, the band gap persists up to 3 GPa. However, the indirect band gap decreases because

additional Fermi pockets approach the Fermi level. The band structure at 4 GPa shown in Fig. 8(c) illustrates that two-hole pockets cross the Fermi level near the Γ -point (Z - A , Y -point) and one electron pocket crosses the Fermi level along the Γ - X direction. The band structure at 6 GPa, Fig. 8, indicates that the bands become more hole-like compared to the lower pressures

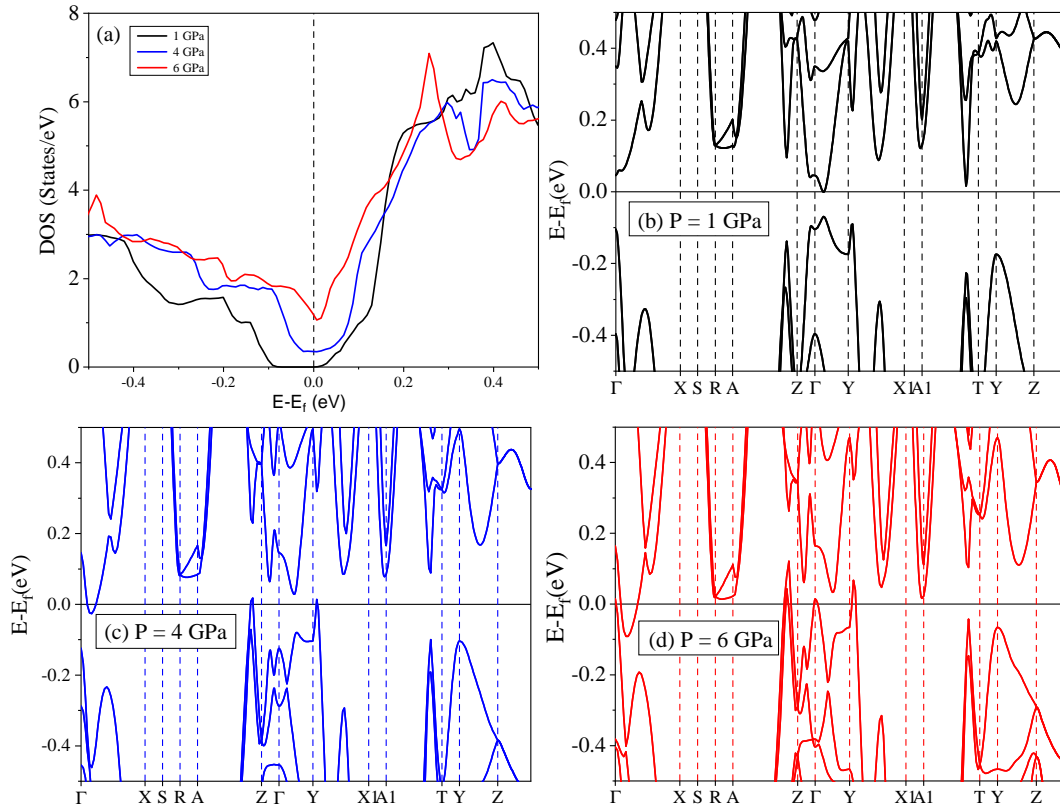


Figure 8. (a) Electronic density of states (DOS) at selected pressure of 1, 4 and 6 GPa. (b)–(d) Band structure at pressures of 1, 4, and 6 GPa, respectively. Figure 8(b) has been reproduced from our previous study [26]

as the extent of the Fermi pockets increases at the Fermi level.

IV. DISCUSSION

The effect of pressure on the electronic properties of transition metal pentatellurides ($ZrTe_5/HfTe_5$) manifests a rich interplay between the band topology, carrier dynamics and superconductivity consistent with the general trend observed in other well-known topological materials like Bi_2Te_3 , Cd_3As_2 , WTe_2 etc[4, 5, 7–9, 13]. Superconductivity in these materials generally coincides with or triggered by the instabilities in its electronic or lattice structure. In the present work, our comprehensive transport and computational results for the CVT grown $ZrTe_5$ single crystals displays a pressure induced transition, leading to pronounced Fermi surface reconstruction and ultimately the superconductivity. At ambient pressure, $ZrTe_5$ displays a characteristic peak in resistivity consistent with the previous reports[32]. However, on application of pressure we observe a significant non-monotonic change in position

and magnitude of resistivity peak. More importantly, in between 5 to 6 GPa pressure, the resistivity peak disappears completely indicating the pressure induced reconstruction of underlying electronic band structure. The concomitant change in residual resistivity under pressure, further highlights the impact of high pressure on scattering phenomenon. The immediate evidence of the Fermi surface reconstruction comes from our pressure dependent magnetotransport experiments (MR and Hall resistivity, Fig. 13 & 14). There is a huge suppression in MR compared to our ambient pressure study of same samples[32]. Approximately linear field dependence of MR and Hall resistivity in low pressure regime (1-3 GPa) points to a simple, electron dominated transport, while in the intermediate pressure regime (4-6 GPa) non-linearity emerges in both MR and Hall resistivity indicates the participation of holes along with the electrons i.e. multi-band transport. This feature is quantitatively confirmed by the analysis of carrier density (n) and mobility (μ) extracted from two carrier model [Eq. 2] revealing a systematic pressure induced increase of hole concentration. The electronic structure of $ZrTe_5$ is known to host multiple electron and hole pockets, especially under applied pressure [24], but here

we employ a simplified two-band model as an effective empirical description of the magnetotransport. This approach is commonly used to identify the dominant conduction channels in topological semimetals [41], where it reliably captures the essential features of Hall and magnetoresistance data even in the presence of multiple bands. The extracted carrier densities and mobilities thus represent effective transport parameters explaining the pressure-induced evolution of the system. It is clear from Figure 9 that this system evolves from the electron dominated band at low temperature to the nearly perfect electron hole compensated band at 6 GPa, causing the extreme magnetoresistance (XMR) ~ 1400 %. The sign reversal of the Hall resistivity, confirms a crossover from electron to hole dominated band beyond 6 GPa, with linear positive slope is recovered by 7 GPa [Fig. 5(g)].

Our experimental observations are well supported by first-principles density functional theory (DFT) calculations. At ambient pressure, the conduction and valence bands nearly touch at the Γ point, producing a Dirac-like dispersion as a result of an accidental Dirac semimetal state [22, 26, 42], in agreement with the observed non-trivial Berry phase reported previously by us and other groups [26, 27]. In low pressure regime (1–3 GPa), the calculations reveal a small band gap opening (Band wrapping) at Γ point, consistent with the resistivity enhancement. More critically, on further raising pressure the calculation results in increased density of states at the Fermi level along with the emergence of multiple Fermi pockets origination at the Γ point, along the Γ -X, A-Z and Y-X directions. The systematic band evolution in this study supports a critical change in the electronic band structure of ZrTe_5 under pressure, explaining the multiband conduction and providing the relation between the electronic structure modification and experimentally observed phenomenon. This dramatic electronic instability under pressure may be intimately linked to a structural transformation reported by Zhou *et al.* near 6 GPa [25]. Beyond this pressure, we expect the system to enter into new high-pressure phase which triggers the finally observed phenomenon i.e. the superconductivity at 8 GPa with $T_c \sim 1.8$ K. Here, we observed the emergence of superconductivity 8 GPa, which differs nearly by 2 GPa from the critical pressure for superconductivity as reported by Zhou *et al.* (~ 6 GPa) [25]. This discrepancy likely arises from the combination of experimental and intrinsic sample dependent factors. First, in both the cubic anvil cell (CAC) and diamond anvil cell (DAC), the applied pressure typically decreases upon cooling. Therefore, a pressure difference of approximately ~ 2 GPa is plausible, considering that Zhou *et al.* performed pressure calibration at room temperature, whereas our calibration was carried out at low temperature. In addition, the use of different pressure-transmitting media (glycerol versus Daphne 7373), each with distinct hydrostatic limits, may introduce a minor calibration

offset. Apart from this, ZrTe_5 is highly sensitive to synthesis conditions, as evidenced by the wide variation in ambient-pressure transport properties reported across different studies [26, 32]. To further examine this aspect, we measured the temperature-dependent resistivity (ρ - T) of flux-grown ZrTe_5 crystals under conditions similar to those used in the present work. These measurements reveal a superconducting transition near 7 GPa with a critical temperature $T_c \approx 3.4$ K (Appendix A), highlighting the crucial role of sample quality in stabilizing superconductivity. Taken together, these factors are likely relevant in accounting for the observed discrepancy in the superconducting transition temperature between the two studies. In Figure 3 & 4, the magnetotransport results at 7–8 GPa pressure is presented. The deterioration of the magneto transport signal quality after 6 GPa may likely be a consequence of structural or superconducting transition; however, the similarity between 1.5 K and 5 K data at 8 GPa rules out this possibility. We therefore believe it is due to experimental limitation of high pressure cell or the pressure transmitting medium. The emergence of superconductivity in the vicinity of the structural phase transition strongly suggests an intimate correlation between the pairing mechanism and underlying electronic structure.

V. CONCLUSION

In the present work, we have studied the effect of high pressure on the magnetotransport properties of CVT-grown ZrTe_5 single crystals. Resistivity measurements under varying pressures (0–8 GPa) reveal a non-monotonic and significant shift in the resistivity peak (T_p) and its eventual disappearance at 6 GPa. A superconducting transition is observed at 8 GPa with $T_c=1.8$ K. Our experimental results reveal a pressure-induced electronic transition, as evidenced by drastic change in transport and magnetotransport properties near 6 GPa. Between 4–6 GPa, the hole density increases while the electron density decreases, which suggests the pressure induced reconstruction of electronic bands. At 6 GPa, a nearly balanced carrier population potentially explains the emergence of a dramatic MR of ~ 1400 % at 8 T. Additionally, complementary density functional theory calculations support our experimental findings, showing a substantial pressure-induced change in the density of states, leading to the emergence of multiple electron and hole pockets at the Fermi level. These findings suggest that pressure plays a significant role in driving the electronic transition along with the structural transition, and promoting the emergence of superconductivity in ZrTe_5 . These observations deepen our understanding of pressure regulation on topological systems and provide a pathway for exploring novel quantum states.

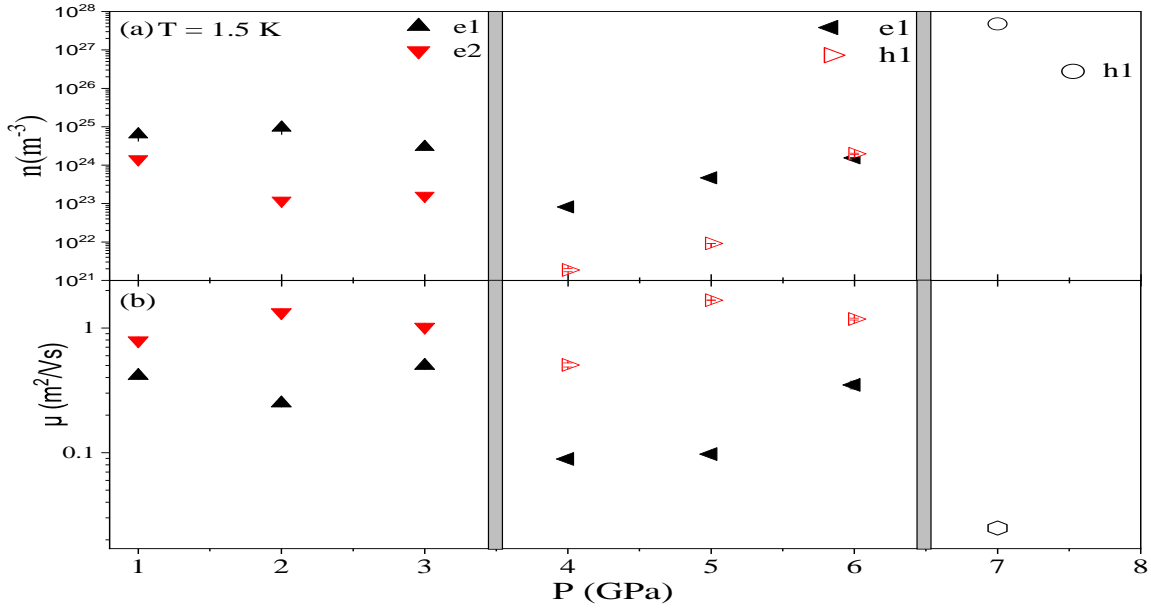


Figure 9. (a) Density and (b) mobility of carriers as function of pressure at 1.5 K, extracted by fitting of Hall conductivity using the one-band or two-carrier models.

VI. ACKNOWLEDGMENTS

S.M. acknowledges the support from the Science and Engineering Research Board (SERB), India, for the Junior Research Fellowship (File No.-SRG/2019/001187). V.K.G. acknowledges to the SERB India for the award of the SERB International Research Experience (SIRE) fellowship (File No.- SIR/2022/000804). P.S. acknowledges to the SERB India for the award of the Start-up research grant (SRG/2019/001187), University Grant Commission (UGC) for Basic Scientific Research (BSR) fund (UGC File No.- 30-505/2020(BSR)), UGC-DAE Centre for providing the fund (CRS/2021-22/01/415) and SERB India for SERB-SIRE fellowship (File No.-SIR/2022/000752). J.G.C. is supported by the National Key Research and Development Program of China (2023YFA1406100, 2021YFA1400200), the National Natural Science Foundation of China (12025408, U23A6003), and CAS PIFI program (2024PG0003).

VII. APPENDIXES

Appendix A

Resistivity Measurements of Flux-Grown ZrTe_5 at 1 and 7 GPa

To support the claim that the superconducting critical pressure (P_c) in ZrTe_5 crystals varies between different crystal batches, we present complementary resistivity data obtained from flux-grown ZrTe_5 crystals [Fig. 10]. The details of synthesis and structural parameters has

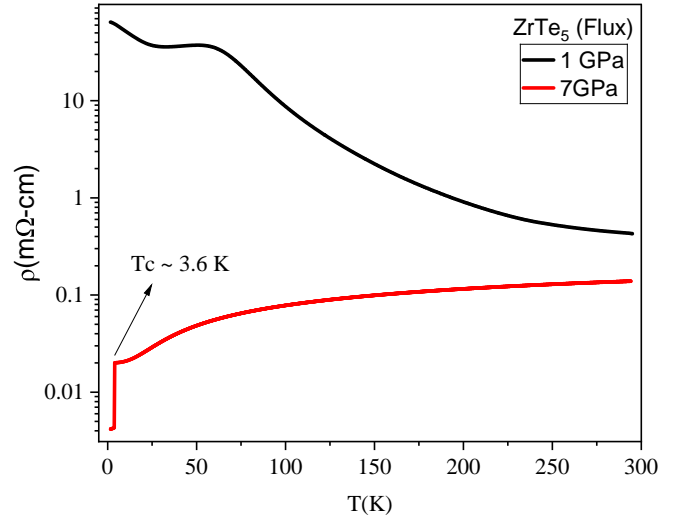


Figure 10. (Appendix A) Pressure-dependent resistivity as a function of temperature for flux-grown ZrTe_5 at 1 and 7 GPa

been reported in Shahi *et al.* [32]. The measurements were carried out under identical experimental conditions to those described in the main text.

Appendix B

Raw magnetotransport data and symmetrization/antisymmetrization procedure

The raw data were measured under both positive and negative magnetic fields (Fig. 11). From these measure-

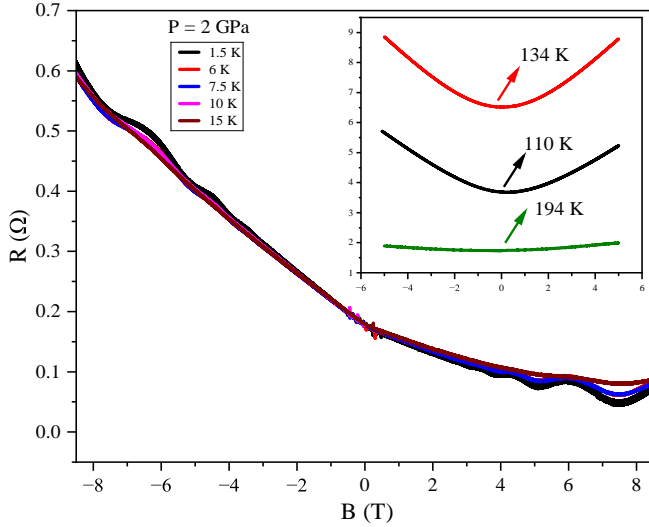


Figure 11. (Appendix B) Raw magnetotransport data at a pressure of 2 GPa prior to symmetrization and anti-symmetrization. The main panel shows data in the low-temperature regime (1.5–15 K), while the inset displays the high-temperature regime (134–194 K).

ments, the even and odd magnetic-field components were separated using the standard relations shown below B2:

$$R_{xx}(B) = \frac{R(+B) + R(-B)}{2}, \quad (\text{B1})$$

$$R_{xy}(B) = \frac{R(+B) - R(-B)}{2}. \quad (\text{B2})$$

In order to minimize possible hysteresis and instrumental effects, both forward and backward magnetic-field sweeps were averaged prior to the symmetrization and antisymmetrization procedures. Interpolation was applied to ensure that the resistance values at $+B$ and $-B$ correspond to identical magnetic field magnitudes, as required for accurate symmetrization and antisymmetrization.

Appendix C

Hall conductivity σ_{xy} at different pressures along with fitting curves using the two-band model.

In Fig. 12, we present the Hall conductivity σ_{xy} at different pressures in the range of 1–6 GPa. The black curves represent the experimental data, while the red curves correspond to the fitting results obtained using Eq. 2.

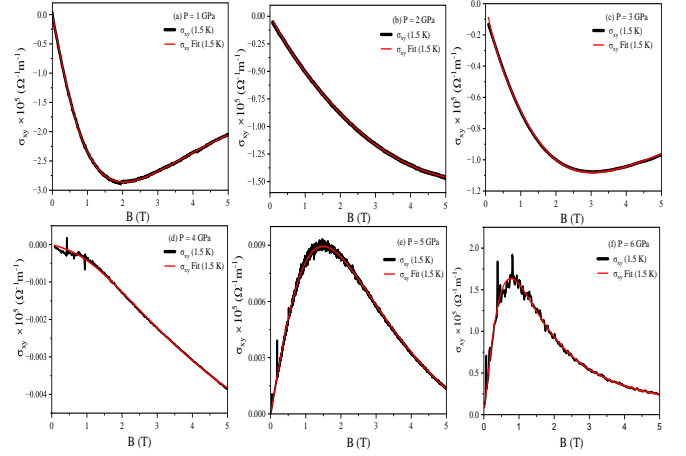


Figure 12. (Appendix C) Hall conductivity σ_{xy} at 1–6 GPa pressure along with the fitting curve shown in Eq. (2)

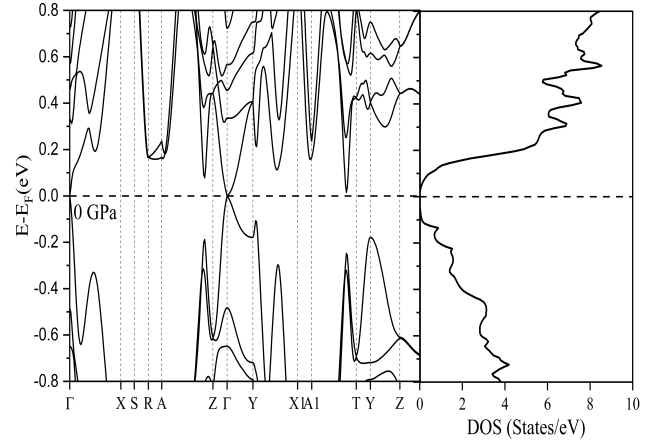


Figure 13. (Appendix D) Bands and DOS of ZrTe_5 at ambient pressure. Reproduced from our recent work [26].

Appendix D

Band structure and Density of states at 0,2,3 and 5 GPa pressure

In order to provide a comprehensive understanding of the effect of pressure on electronic properties of ZrTe_5 , we present the band structure and density of states (DOS) at ambient, 2,3 and 5 GPa pressures, respectively. The Figure 13 & 14 has been reproduced from our recent study [26]. It is clear from Figure 13, that at ambient pressure there is Dirac-like band dispersion at Γ point. As we increase pressure, the Fermi surface undergoes significant modification [Figure (14-16)]. A pronounced band-wrapping can be observed near the Γ , Z and Y points at 2 & 3 GPa pressure [Figure 14, Figure 15]. At 5 GPa pressure two hole pockets and one electron pocket appear to cross the Fermi level.

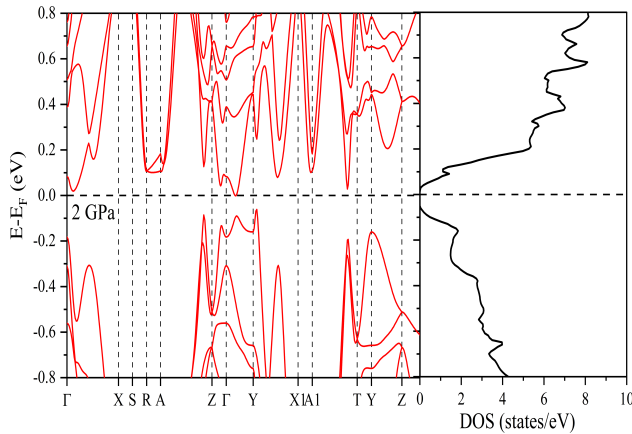


Figure 14. (Appendix D) Bands and DOS of ZrTe_5 at 2 GPa pressure. Reproduced from our recent work [26].

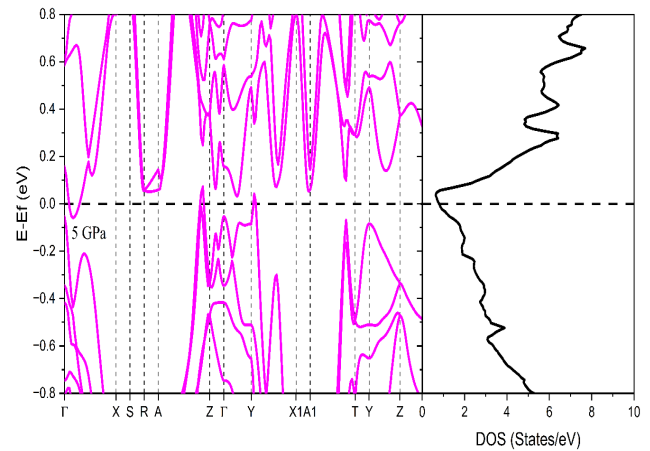


Figure 16. (Appendix D) Bands and DOS of ZrTe_5 at 5 GPa pressure.

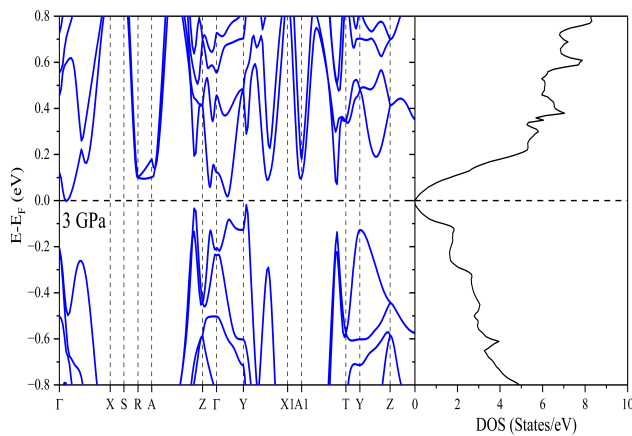


Figure 15. (Appendix D) Bands and DOS of ZrTe_5 at 3 GPa pressure.

-
- [1] Y. Li and Z.-A. Xu, Exploring topological superconductivity in topological materials, [Advanced Quantum Technologies](#) **2**, 1800112 (2019).
 - [2] C. Zhang, L. Sun, Z. Chen, X. Zhou, Q. Wu, W. Yi, J. Guo, X. Dong, and Z. Zhao, Phase diagram of a pressure-induced superconducting state and its relation to the Hall coefficient of Bi_2Te_3 single crystals, [Phys. Rev. B](#) **83**, 140504 (2011).
 - [3] K. Kirshenbaum, P. S. Syers, A. P. Hope, N. P. Butch, J. R. Jeffries, S. T. Weir, J. J. Hamlin, M. B. Maple, Y. K. Vohra, and J. Paglione, Pressure-induced unconventional superconducting phase in the topological insulator Bi_2Se_3 , [Phys. Rev. Lett.](#) **111**, 087001 (2013).
 - [4] J. Zhu, J. L. Zhang, P. P. Kong, S. J. Zhang, X. H. Yu, J. L. Zhu, Q. Q. Liu, X. Li, R. C. Yu, R. Ahuja, W. G. Yang, G. Y. Shen, H. K. Mao, H. M. Weng, X. Dai, Z. Fang, Y. S. Zhao, and C. Q. Jin, Superconductivity in topological insulator Sb_2Te_3 induced by pressure, [Scientific Reports](#) **3**, 2016 (2013).
 - [5] J. L. Zhang, S. J. Zhang, H. M. Weng, W. Zhang, L. X. Yang, Q. Q. Liu, S. M. Feng, X. C. Wang, R. C. Yu, L. Z. Cao, L. Wang, W. G. Yang, H. Z. Liu, W. Y. Zhao, S. C. Zhang, X. Dai, Z. Fang, and C. Q. Jin, Pressure-induced superconductivity in topological parent compound Bi_2Te_3 , [Proceedings of the National Academy of Sciences](#) **108**, 24 (2011).
 - [6] L. He, Y. Jia, S. Zhang, X. Hong, C. Jin, and S. Li, Pressure-induced superconductivity in the three-dimensional topological Dirac semimetal Cd_3As_2 , [npj Quantum Materials](#) **1**, 16014 (2016).
 - [7] D. Kang, Y. Zhou, W. Yi, C. Yang, J. Guo, Y. Shi, S. Zhang, Z. Wang, C. Zhang, S. Jiang, A. Li, K. Yang, Q. Wu, G. Zhang, L. Sun, and Z. Zhao, Superconductivity emerging from a suppressed large magnetoresistant state in tungsten ditelluride, [Nature Communications](#) **6**, 7804 (2015).
 - [8] Y. Qi, P. G. Naumov, M. N. Ali, C. R. Rajamathi, W. Schnelle, O. Barkalov, M. Hanfland, S.-C. Wu,

- C. Shekhar, Y. Sun, V. Süß, M. Schmidt, U. Schwarz, E. Pippel, P. Werner, R. Hillebrand, T. Förster, E. Kampert, S. Parkin, R. J. Cava, C. Felser, B. Yan, and S. A. Medvedev, Superconductivity in Weyl semimetal candidate MoTe_2 , *Nature Communications* **7**, 11038 (2016).
- [9] S. Kobayashi and M. Sato, Topological superconductivity in Dirac Semimetals, *Phys. Rev. Lett.* **115**, 187001 (2015).
- [10] Y. Li, C. An, C. Hua, X. Chen, Y. Zhou, Y. Zhou, R. Zhang, C. Park, Z. Wang, Y. Lu, Y. Zheng, Z. Yang, and Z.-A. Xu, Pressure-induced superconductivity in topological semimetal NbAs_2 , *npj Quantum Materials* **3**, 58 (2018).
- [11] J. Nayak, S.-C. Wu, N. Kumar, C. Shekhar, S. Singh, J. Fink, E. E. D. Rienks, G. H. Fecher, S. S. P. Parkin, B. Yan, and C. Felser, Multiple Dirac cones at the surface of the topological metal LaBi , *Nature Communications* **8**, 13942 (2017).
- [12] B. Q. Lv, Z.-L. Feng, Q.-N. Xu, X. Gao, J.-Z. Ma, L.-Y. Kong, P. Richard, Y.-B. Huang, V. N. Strocov, C. Fang, H.-M. Weng, Y.-G. Shi, T. Qian, and H. Ding, Observation of three-component fermions in the topological semimetal molybdenum phosphide, *Nature* **546**, 627 (2017).
- [13] Z. Chi, X. Chen, C. An, L. Yang, J. Zhao, Z. Feng, Y. Zhou, Y. Zhou, C. Gu, B. Zhang, Y. Yuan, C. Kenney-Benson, W. Yang, G. Wu, X. Wan, Y. Shi, X. Yang, and Z. Yang, Pressure-induced superconductivity in MoP , *npj Quantum Materials* **3**, 28 (2018).
- [14] H. Weng, X. Dai, and Z. Fang, Transition-metal pentatelluride ZrTe_5 and HfTe_5 : A paradigm for large-gap quantum spin hall insulators, *Phys. Rev. X* **4**, 011002 (2014).
- [15] S. Okada, T. Sambongi, and M. Ido, Giant resistivity anomaly in ZrTe_5 , *Journal of the Physical Society of Japan* **49**, 839 (1980).
- [16] T. Jones, W. Fuller, T. Wieting, and F. Levy, Thermoelectric power of HfTe_5 and ZrTe_5 , *Solid State Communications* **42**, 793 (1982).
- [17] Q. Li, D. E. Kharzeev, C. Zhang, Y. Huang, I. Pletikosić, A. V. Fedorov, R. D. Zhong, J. A. Schneeloch, G. D. Gu, and T. Valla, Chiral magnetic effect in ZrTe_5 , *Nature Physics* **12**, 550 (2016).
- [18] T. Liang, J. Lin, Q. Gibson, S. Kushwaha, M. Liu, W. Wang, H. Xiong, J. A. Sobota, M. Hashimoto, P. S. Kirchmann, Z.-X. Shen, R. J. Cava, and N. P. Ong, Anomalous Hall effect in ZrTe_5 , *Nature Physics* **14**, 451 (2018).
- [19] J. L. Zhang, C. M. Wang, C. Y. Guo, X. D. Zhu, Y. Zhang, J. Y. Yang, Y. Q. Wang, Z. Qu, L. Pi, H.-Z. Lu, and M. L. Tian, Anomalous thermoelectric effects of ZrTe_5 in and beyond the quantum limit, *Phys. Rev. Lett.* **123**, 196602 (2019).
- [20] W. Zhang, P. Wang, B. Skinner, R. Bi, V. Kozii, C.-W. Cho, R. Zhong, J. Schneeloch, D. Yu, G. Gu, L. Fu, X. Wu, and L. Zhang, Observation of a thermoelectric Hall plateau in the extreme quantum limit, *Nature Communications* **11**, 1046 (2020).
- [21] Y. Wang, H. F. Legg, T. Bömerich, J. Park, S. Biesenkamp, A. A. Taskin, M. Braden, A. Rosch, and Y. Ando, Gigantic magnetochiral anisotropy in the topological semimetal ZrTe_5 , *Phys. Rev. Lett.* **128**, 176602 (2022).
- [22] Z. Fan, Q.-F. Liang, Y. B. Chen, S.-H. Yao, and J. Zhou, Transition between strong and weak topological insulator in ZrTe_5 and HfTe_5 , *Scientific Reports* **7**, 45667 (2017).
- [23] Y. Liu, Y. J. Long, L. X. Zhao, S. M. Nie, S. J. Zhang, Y. X. Weng, M. L. Jin, W. M. Li, Q. Q. Liu, Y. W. Long, R. C. Yu, C. Z. Gu, F. Sun, W. G. Yang, H. K. Mao, X. L. Feng, Q. Li, W. T. Zheng, H. M. Weng, X. Dai, Z. Fang, G. F. Chen, and C. Q. Jin, Superconductivity in HfTe_5 across weak to strong topological insulator transition induced via pressures, *Scientific Reports* **7**, 44367 (2017).
- [24] Z. Kovács-Krausz, D. Nagy, A. Márfy, B. Karpiak, Z. Tajkó, L. Oroszlány, J. Koltai, P. Nemes-Incze, S. P. Dash, P. Makk, S. Csonka, and E. Tóvári, Signature of pressure-induced topological phase transition in ZrTe_5 , *npj Quantum Materials* **9**, 76 (2024).
- [25] Y. Zhou, J. Wu, W. Ning, N. Li, Y. Du, X. Chen, R. Zhang, Z. Chi, X. Wang, X. Zhu, P. Lu, C. Ji, X. Wan, Z. Yang, J. Sun, W. Yang, M. Tian, Y. Zhang, and H. Mao, Pressure-induced superconductivity in a three-dimensional topological material ZrTe_5 , *Proceedings of the National Academy of Sciences of the United States of America* **113**, 2904 (2016).
- [26] S. Mishra, N. Singh, V. K. Gangwar, R. Walia, M. Kumar, U. B. Singh, D. S. Saini, J. Sun, G. Chen, D. Bhoi, S. Chatterjee, Y. Uwatoko, J. Cheng, and P. Shahi, Effect of pressure on the transport properties and thermoelectric performance of Dirac semimetal ZrTe_5 , *Phys. Rev. B* **112**, 165140 (2025).
- [27] J. L. Zhang, C. Y. Guo, X. D. Zhu, L. Ma, G. L. Zheng, Y. Q. Wang, L. Pi, Y. Chen, H. Q. Yuan, and M. L. Tian, Disruption of the accidental Dirac semimetal state in ZrTe_5 under hydrostatic pressure, *Phys. Rev. Lett.* **118**, 206601 (2017).
- [28] Y. Qi, W. Shi, P. G. Naumov, N. Kumar, W. Schnelle, O. Barkalov, C. Shekhar, H. Borrmann, C. Felser, B. Yan, and S. A. Medvedev, Pressure-driven superconductivity in the transition-metal pentatelluride HfTe_5 , *Phys. Rev. B* **94**, 054517 (2016).
- [29] D. Santos-Cottin, M. Padlewski, E. Martino, S. B. David, F. Le Mardelé, F. Capitani, F. Borondics, M. D. Bachmann, C. Putzke, P. J. W. Moll, R. D. Zhong, G. D. Gu, H. Berger, M. Orlita, C. C. Homes, Z. Rukelj, and A. Akrap, Probing intraband excitations in ZrTe_5 : A high-pressure infrared and transport study, *Phys. Rev. B* **101**, 125205 (2020).
- [30] J.-G. Cheng, B.-S. Wang, J.-P. Sun, and Y. Uwatoko, Cubic anvil cell apparatus for high-pressure and low-temperature physical property measurements*, *Chinese Physics B* **27**, 077403 (2018).
- [31] Y. Uwatoko, K. Matsubayashi, T. Matsumoto, N. Aso, M. Nishi, T. Fujiwara, M. Hondo, S. Tabata, K. Takagi, M. Tawata, and H. Kagi, Development of an ultracompact cubic-anvil pressure apparatus for ultralow temperatures, *High Pressure Research* **18**, 230 (2008).
- [32] P. Shahi, D. J. Singh, J. P. Sun, L. X. Zhao, G. F. Chen, Y. Y. Lv, J. Li, J.-Q. Yan, D. G. Mandrus, and J.-G. Cheng, Bipolar conduction as the possible origin of the electronic transition in pentatellurides: Metallic vs semiconducting behavior, *Phys. Rev. X* **8**, 021055 (2018).
- [33] T. Osakabe and K. Kakurai, Feasibility tests on pressure-transmitting media for single-crystal magnetic neutron diffraction under high pressure, *Japanese Journal of Applied Physics* **47**, 6544 (2008).

- [34] P. Giannozzi, O. Andreussi, T. Brumme, O. Bunau, M. Buongiorno Nardelli, M. Calandra, R. Car, C. Cavazzoni, D. Ceresoli, M. Cococcioni, N. Colonna, I. Carnimeo, A. Dal Corso, S. de Gironcoli, P. Delugas, R. A. DiStasio, A. Ferretti, A. Floris, G. Fratesi, G. Fugallo, R. Gebauer, U. Gerstmann, F. Giustino, T. Gorni, J. Jia, M. Kawamura, H.-Y. Ko, A. Kokalj, E. Küçükbenli, M. Lazzeri, M. Marsili, N. Marzari, F. Mauri, N. L. Nguyen, H.-V. Nguyen, A. Otero-de-la Roza, L. Paulatto, S. Poncé, D. Rocca, R. Sabatini, B. Santra, M. Schlipf, A. P. Seitsonen, A. Smogunov, I. Timrov, T. Thonhauser, P. Umari, N. Vast, X. Wu, and S. Baroni, Advanced capabilities for materials modelling with quantum espresso, *Journal of Physics: Condensed Matter* **29**, 465901 (2017).
- [35] J. P. Perdew, K. Burke, and M. Ernzerhof, Generalized gradient approximation made simple, *Phys. Rev. Lett.* **77**, 3865 (1996).
- [36] S. Grimme, J. Antony, S. Ehrlich, and H. Krieg, A consistent and accurate ab initio parametrization of density functional dispersion correction (dft-d) for the 94 elements h-pu, *The Journal of Chemical Physics* **132**, 154104 (2010).
- [37] Y. Zhang, C. Wang, L. Yu, G. Liu, A. Liang, J. Huang, S. Nie, X. Sun, Y. Zhang, B. Shen, J. Liu, H. Weng, L. Zhao, G. Chen, X. Jia, C. Hu, Y. Ding, W. Zhao, Q. Gao, C. Li, S. He, L. Zhao, F. Zhang, S. Zhang, F. Yang, Z. Wang, Q. Peng, X. Dai, Z. Fang, Z. Xu, C. Chen, and X. J. Zhou, Electronic evidence of temperature-induced lifshitz transition and topological nature in ZrTe_5 , *Nature Communications* **8**, 15512 (2017).
- [38] M. M. Piva, R. Wawrzyńczak, N. Kumar, L. O. Kutelak, G. A. Lombardi, R. D. dos Reis, C. Felser, and M. Nicklas, Importance of the semimetallic state for the quantum hall effect in HfTe_5 , *Phys. Rev. Mater.* **8**, L041202 (2024).
- [39] J. Gao, M. Zhong, Q.-J. Liu, B. Tang, F.-S. Liu, and X.-J. Ma, Effects of pressure on structural, electronic, optical, and mechanical properties of zrte_5 : A density functional theory study, *Physica B: Condensed Matter* **620**, 413286 (2021).
- [40] Y. Zhang, C. Wang, G. Liu, A. Liang, L. Zhao, J. Huang, Q. Gao, B. Shen, J. Liu, C. Hu, W. Zhao, G. Chen, X. Jia, L. Yu, L. Zhao, S. He, F. Zhang, S. Zhang, F. Yang, Z. Wang, Q. Peng, Z. Xu, C. Chen, and X. Zhou, Temperature-induced lifshitz transition in topological insulator candidate HfTe_5 , *Science Bulletin* **62**, 950 (2017).
- [41] G. Eguchi and S. Paschen, Robust scheme for magnetotransport analysis in topological insulators, *Phys. Rev. B* **99**, 165128 (2019).
- [42] G. Manzoni, L. Gragnaniello, G. Autès, T. Kuhn, A. Sterzi, F. Cilento, M. Zacchigna, V. Enenkel, I. Vobornik, L. Barba, F. Bisti, P. Bugnon, A. Margrez, V. N. Strocov, H. Berger, O. V. Yazyev, M. Fonin, F. Parmigiani, and A. Crepaldi, Evidence for a strong topological insulator phase in ZrTe_5 , *Phys. Rev. Lett.* **117**, 237601 (2016).